

Quasiparticle and Optical Properties of Rutile and Anatase TiO₂

Wei Kang and Mark S. Hybertsen

Center for Functional Nanomaterials, Brookhaven National Laboratory, Upton, NY 11973

(Dated: June 23, 2021)

Quasiparticle excitation energies and optical properties of TiO₂ in the rutile and anatase structures are calculated using many-body perturbation theory methods. Calculations are performed for a frozen crystal lattice; electron-phonon coupling is not explicitly considered. In the GW method, several approximations are compared and it is found that inclusion of the full frequency dependence as well as explicit treatment of the Ti semicore states are essential for accurate calculation of the quasiparticle energy band gap. The calculated quasiparticle energies are in good agreement with available photoemission and inverse photoemission experiments. The results of the GW calculations, together with the calculated static screened Coulomb interaction, are utilized in the Bethe-Salpeter equation to calculate the dielectric function $\epsilon_2(\omega)$ for both the rutile and anatase structures. The results are in good agreement with experimental observations, particularly the onset of the main absorption features around 4 eV. For comparison to low temperature optical absorption measurements that resolve individual excitonic transitions in rutile, the low-lying discrete excitonic energy levels are calculated with electronic screening only. The lowest energy exciton found in the energy gap of rutile has a binding energy of 0.13 eV. In agreement with experiment, it is not dipole allowed, but the calculated exciton energy exceeds that measured in absorption experiments by about 0.22 eV and the scale of the exciton binding energy is also too large. The quasiparticle energy alignment of rutile is calculated for non-polar (110) surfaces. In the GW approximation, the valence band maximum is 7.8 eV below the vacuum level, showing a small shift from density functional theory results.

PACS numbers: 71.20.Nr 71.15.Qe 71.35.Cc

I. INTRODUCTION

Even after half a century of research^{1,2}, investigation of the fundamental properties of titanium dioxide (TiO₂) crystal phases remains important and fruitful, in part due to the role they have in concepts to effectively utilize solar energy. For example, TiO₂ structures form the photoactive component in heterogeneous photo-catalysts which, by absorbing energy from the sunlight, degrade environmentally hazardous materials^{3,4} and split water into H₂ and O₂⁵. Scintered anatase TiO₂ nanoparticles provide the backbone for electron transport and the substrate for organic chromophores in the Grätzel photovoltaic solar cells⁶. In addition to that, TiO₂ has been widely used in various areas from optical coatings to pigments². Fundamental to all of these applications are the relative alignments of essential energy levels near the valence and conduction band edges of TiO₂ crystal phases and the corresponding optical transition energies. If predictive computational methods are going to have impact on the understanding and design of heterogeneous photocatalytic systems based on TiO₂, we must first establish that these methods can predict the basic properties of the crystal phases, providing a coherent framework for all the experimental facts.

Rutile and anatase are two common crystal structures in which TiO₂ is found. In both phases, each Ti atom in the crystal is surrounded by a slightly distorted octahedron formed by six oxygen atoms. The distinct phases exhibit a different connection between the distorted octahedra (TiO₆). In the rutile phase each octahedron shares two edges with its neighbors, while in the anatase phase

each octahedron shares four⁷. In the rutile form, the crystal has a simple-tetragonal structure⁸ with $a = b = 0.45936$ nm and $c = 0.29587$ nm. The symmetry of the lattice is described by the space group $P4_2/mnm$ with the only internal parameter $u = 0.30479$. In the anatase form the crystal structure is body-centered tetragonal^{9,10} and belongs to space group $I4_1/amd$. The three sides of the conventional cell are $a = b = 0.3784$ nm and $c = 0.9515$ nm respectively. The internal parameter u is $0.208^{9,10}$. The measurements quoted were done at room temperature; the change in lattice parameters upon reducing the temperature to 15 K is less than 0.001 nm¹¹.

Most of the early first-principles calculations of the properties of TiO₂ were based on the local density approximation (LDA) in a Density Functional Theory (DFT) based approach^{12,13}. The crystal structures and ground-state properties were accurately reproduced¹⁴⁻¹⁷. However, as has been more generally observed for semiconductors and insulators, the energy gaps pertaining to optical properties were found to be too small. The minimum energy gap in the LDA band structure underestimated the band gap observed in optical experiments^{18,19} by about 40%¹⁶. Calculations based on Hartree-Fock theory have been performed, giving accurate structural properties for rutile and anatase, but with a minimum energy gap that exceeded 10 eV¹⁰. A hybrid approach, admixing a fraction of the bare exchange from Hartree-Fock, also showed accurate structural properties for rutile²⁰, with a band gap that is closer to experiment (3.4 eV)²¹. A more economical approach, approximately accounting for explicit Coulomb interactions through a U parameter acting on the Ti 3d electrons in a DFT+ U

approach, overestimated the lattice parameters while still showing a band gap that was smaller than experiment²².

A direct approach to calculate electronic excitation energies based on the Green's function approach of many-body perturbation theory (MBPT), specifically utilizing the GW approximation for the electron self energy²³, has proven to be relatively accurate for a broad array of materials²⁴⁻²⁷. Several calculations have been reported for TiO₂ with different implementations of the GW method²⁸⁻³¹. However, the band gap was significantly overestimated in all these reports.

The frequency dependent macroscopic dielectric function probed in optical measurements has been extensively studied within the framework of DFT for TiO₂ crystal phases^{14,15,17,32}. Using the independent particle approach of Ehrenreich and Cohen³³, the underestimate of the fundamental band gap immediately gives an error in the optical threshold and the overall shape of the dielectric function calculated in this way was quite different from the experimental measurements^{34,35}. In the framework of MBPT, the GW-based results for the electronic excitation energies are input to a direct treatment of neutral excitations through solution of the two-particle Bethe-Salpeter equation (BSE), an approach that has provided a satisfactory description of the optical properties of a number of systems^{27,36}. An application of the BSE approach for rutile and anatase TiO₂ has only recently appeared in the literature³⁷. The shape of the spectra are in much better agreement with experiment as compared to the independent particle approach.

In this article, we critically assess the application of MBPT methods to calculate the electronic and optical excitations for TiO₂ in the rutile and anatase crystal phases. To treat the electronic excitation energies, we use the GW method without self consistency or inclusion of vertex corrections. Empirically, this approach is often relatively accurate, although a full understanding of cancellations between self consistency and vertex corrections remains an open area of research³⁸⁻⁴⁴. Several different approximations to handle the frequency dependence of the screened Coulomb interaction in the GW method are compared. We find that use of plasmon pole models^{24,45} results in significant overestimation of the band gap. When the full frequency dependence of the screening is included, together with explicit treatment of the Ti semicore states, the calculated electronic excitation spectrum is found to be in good agreement with photoemission and inverse photoemission spectra^{46,47}. Interestingly, the calculated fundamental gap (3.34 eV and 3.56 eV for rutile and anatase respectively), is still larger than the measured minimum gap from optical absorption (3.03 eV for rutile¹⁸ and estimated to be 3.3 eV for anatase¹⁹). As a first step towards application to heterogeneous photocatalytic systems, we discuss the alignment of the valence and conduction band edges at non-polar vacuum-solid (110) interface of TiO₂. We find that the GW method implies only very small corrections relative to the LDA for the valence band position, with the most

of the band gap error going to shift the conduction band edge upwards.

To explore the role of electron-hole interactions and excitonic binding energy, we have used the results from the GW based calculations as input to the BSE approach. Similar to the recent results of Lawler *et al.*³⁷, the calculated frequency dependent dielectric function accurately reproduces the main onset of absorption near 4 eV and gives a good account of the frequency dependence for both rutile and anatase. We also solve the BSE for the low-lying, bound exciton states for rutile. The deepest exciton binding energy is calculated to be about 0.13 eV. The dipole-forbidden character of the lowest exciton agrees with low temperature measurements¹⁸, although the predicted exciton energy (3.25 eV) is still 0.22 eV larger than experiments. Also, the magnitude of the exciton binding energy is larger. While the discrepancy for the exciton energy could very reasonably be regarded as within the expected errors of the MBPT methods used here, it may suggest an important role for electron-phonon coupling in screening and in further renormalizing the energy gap in TiO₂.

The rest of the article is organized as follows: In Sec. II, the methodologies used in the DFT, electronic excitation and optical excitation calculations are briefly summarized, the key approximations are discussed and the numerical details are provided. In Sec. III, we present the main results for the electronic and optical excitations in rutile and anatase TiO₂ and discuss them in comparison to available experiments. Finally, we conclude the article in Sec. IV with a short discussion, including the role of coupling to phonons.

II. METHODOLOGY AND NUMERICAL DETAILS

A. DFT Calculations

The LDA eigenvalues and eigenvectors of TiO₂ are calculated with a plane-wave basis set using norm-conserving pseudopotentials. Unless indicated otherwise, the LDA calculations are carried out using the ABINIT package^{48,49}. In TiO₂ the Ti is nominally ionized to [Ti⁴⁺] and the low lying conduction band states are of predominantly 3*d* character. As we show below, artificially dividing the n=3 shell of Ti into frozen core (3*s* and 3*p*) and valence (3*d*) contributions introduces a significant error to the energy band gap. The pseudopotential of Ti which includes semicore electrons is generated using the OPIUM package⁵⁰ in the Troullier-Martins scheme⁵¹ with an initial configuration of $(Ne)3s^23p^63d^04s^04p^0$. The outermost five orbitals are included and the cutoff radii (in Bohr) are 0.9, 0.9, 1.0, 0.9, and 0.9 respectively. Other pseudopotentials are taken from the ABINIT pseudopotential database generated using the FHI99PP package⁵².

In all calculations, the Perdew-Wang representation⁵³

of Ceperly-Alder exchange-correlation potential⁵⁴ is used. When including the Ti semicore states, a kinetic energy cutoff of 200 Ry is used to ensure the convergence of the LDA results, as suggested by previous calculations^{16,55}. To examine the accuracy of the pseudopotentials, we calculate the optimized lattice constants for rutile, finding $a = 4.5484 \text{ \AA}$ (4.5936 \AA), $c/a = 0.6414$ (0.64409) and $u = 0.3040$ (0.30479), agreeing with the experimental values noted in parentheses⁸ to the accuracy generally expected for LDA calculations. We also compare our LDA calculations with results obtained using the VASP package^{56,57} with the recommended projector augmented-wave (PAW) pseudopotentials⁵⁸. The difference between the two LDA calculations is within 0.5% for lattice parameters and less than 0.05 eV for bandgaps. In the GW and BSE calculations described below, the geometrical parameters of the unit cell for both rutile and anatase phases are taken from experimental measurements^{8-10,59}.

B. GW Method

In MBPT, the evolution of the electrons in a material is described by the one-particle Green's function, with the effect of electron-electron interactions represented by an electron self energy operator. Well defined electronic excitations appear as peaks in the corresponding spectral function. Excitations with single particle character, namely quasiparticles, can be obtained as solutions of a Schrodinger-like equation⁶⁰

$$(T + V_{ext} + V_H)\psi_{n,k}(\mathbf{r}) + \int d\mathbf{r}' \Sigma(\mathbf{r}, \mathbf{r}'; E_{n,k})\psi_{n,k}(\mathbf{r}') = E_{n,k}\psi_{n,k} \quad (1)$$

where T is the kinetic energy, V_{ext} is the external potential, and V_H is the average Hartree potential. Σ is the self energy of the electrons and the indices refer to Bloch states n, k . It includes all the exchange-correlation effects contributed by surrounding electrons. Since Σ is generally non-Hermitian, $E_{n,k}$ is complex with the real part giving the quasiparticle energy and the imaginary part corresponding to the width of the quasiparticle peak in the spectral function, i.e. the quasiparticle lifetime.

A practical approximation to calculate Σ has proven to be the so-called GW approximation of Hedin²³, in which the self energy $\Sigma(\mathbf{r}, \mathbf{r}'; E)$ is formally written as

$$\Sigma(\mathbf{r}, \mathbf{r}'; E) = \frac{i}{2\pi} \int dE' e^{-i\delta^+ E'} G(\mathbf{r}, \mathbf{r}'; E - E') W(\mathbf{r}, \mathbf{r}'; E'), \quad (2)$$

Here G is the Green's function of the electrons and W is the dynamically screened Coulomb interaction determined by the inverse dielectric matrix $\epsilon^{-1}(\mathbf{r}, \mathbf{r}''; E)$, and δ^+ is a positive infinitesimal time. The G and W in Eq. (2) refer to the fully interacting Green's function. However, in practice, using an initial LDA calculation to determine the screening through linear response calculations (not including the exchange-correlation kernel) and to provide an initial, independent-particle Green's function has often proven to be sufficiently accurate. There are specific examples where the LDA orbital character can be wrong, e.g. in some late 3d transition metal compounds⁶¹⁻⁶³. However, in TiO_2 , the Ti 3d is almost empty and the valence band edge region is predominantly O 2p character with minimal admixture of Ti 3d. The TiO_2 case should be similar to the vast majority of semiconductors and insulators in this regard. Also, the LDA wavefunctions are sufficiently accurate that a first order estimate of the self energy correction to the LDA eigenvalues is adequate. The quasiparticle energy correction $\Delta E_{n,k}$ to a LDA orbital $\phi_{n,k}$ is obtained through a reduced form of Eq. (1) as

$$\Delta E_{n,k} = Z_{n,k} \langle \phi_{n,k} | \Sigma(E_{n,k}^{LDA}) - V_{xc}^{LDA} | \phi_{n,k} \rangle, \quad (3)$$

where V_{xc}^{LDA} is the exchange-correlation potential and $Z_{n,k}$ is the renormalization factor of the orbital defined as $Z_{n,k} = (1 - \partial\Sigma/\partial E)^{-1}|_{E=E_{n,k}^{LDA}}$.

The frequency dependence of the screened Coulomb interaction (W) can often be addressed using a generalized plasmon-pole (GPP) model^{24,45}, with substantial advantages in computational efficiency. The GPP models have proven to be relatively accurate for many semiconductors and insulators, including ionic crystals such as LiCl ⁶⁴ and MgO ⁶⁵. However, as discussed below, we find that use of the GPP leads to a gap that is substantially too large for TiO_2 . Several approaches to include the full frequency-dependent dielectric matrix have been implemented and described in the literature: (1) an analytical continuation method^{66,67}, (2) a direct method which carries out the integration in Eq. (2) along the real axis⁶⁸⁻⁷⁰, and (3) a contour deformation (CD) method which deforms the integration in Eq. (2) along the imaginary axis⁷¹. We adopt the contour deformation method to carry out the calculations, which is particularly efficient for evaluating self energy for states near the gap region.

In the CD method, the correlation contribution $\Sigma^c(\mathbf{r}, \mathbf{r}'; E)$ of the self energy is written as the sum of two terms^{71,72}

$$\Sigma^c(\mathbf{r}, \mathbf{r}'; E) = - \sum_{n,k} \phi_{n,k}(\mathbf{r}) \phi_{n,k}^*(\mathbf{r}') \left\{ \frac{1}{\pi} \int_0^\infty dE'' \frac{E - E_{n,k}}{(E - E_{n,k})^2 + E''^2} W_p(\mathbf{r}, \mathbf{r}', iE'') \right.$$

$$+ W_p(\mathbf{r}, \mathbf{r}'; |E - E_{n,k}| - i\eta) [\Theta(E_f - E_{n,k})\Theta(E_{n,k} - E) - \Theta(E_{n,k} - E_f)\Theta(E - E_{n,k})], \quad (4)$$

where $W_p = W - V_{coul}$, E_f is the Fermi energy, η is a small damping amplitude and Θ is a Heaviside function. The first term in Eq. (4) comes from the integration along the imaginary axis. As W is now smooth along the imaginary axis, a sparse sampling of E is sufficient to converge the integration. The second term is the residual contribution of poles near the real axis. It is non-zero only while $E > E_{n,k} > E_f$ or $E < E_{n,k} < E_f$. For any E close to the Fermi surface, only W_p for $|E - E_{n,k}| \sim 0$ have non-vanished contributions to Σ^c in the second term. This makes the calculation more computational efficient; W is a smooth function of $|E - E_{n,k}|$ around 0, due to the band gap, and only relatively low frequencies need to be sampled.

We implement the contour deformation approach based on a private branch of the YAMBO package⁷³. The integration along the imaginary axis in Eq. (4) is performed with a non-uniform mesh of N points according to

$$E_i'' = E_0 \tan\left(\frac{i-1}{2N}\pi\right), \quad i = 1, 2, \dots, N, \quad (5)$$

which maps the integration along the imaginary axis to an integration on the $[0, 1)$ interval. The energy E_0 provides a scale for the overall density of the samples on the imaginary axis. Half of the mesh spans the energy scale from zero up to E_0 while the other half sample the higher energies. For TiO_2 , a mesh of 50 points and an energy scale of 1 Ry were enough to keep the numerical error of the integration within 1 meV. W_p on the real axis is uniformly sampled with an energy increment of 0.1 eV and values between mesh points are linearly interpolated. The special case in Eq. (4) for $E \rightarrow E_{n,k}$ must be handled with care. A consistent treatment, that avoids the apparent divergence and properly handles all the terms in Eq. (4), is to add a small positive energy to $E - E_{n,k}$ (say $\delta = 2.0 \times 10^{-7}$ Ry) when necessary. A very similar contour deformation approach has been implemented in ABINIT⁷², and we have carefully compared the results for test cases. The ABINIT package has also been used for the GPP model calculations.

For all the GW calculations, the energy cutoff is 60 Ry for the evaluation of the bare Coulomb exchange contribution Σ_x , and 20 Ry for the correlation part Σ_c . A total of 160 bands are used for the calculation of both dielectric matrices and self-energies. An unshifted $4 \times 4 \times 6$ Monkhost-Pack (MP) mesh⁷⁴ is used to sample the Brillouin zone (BZ) of rutile, while for anatase an unshifted $4 \times 4 \times 4$ MP mesh is used.

A test of the convergence with respect to the number of bands included is shown in Fig. 1 for the final full-frequency approach with Ti semicore electrons treated explicitly as valence electrons in the pseudopo-

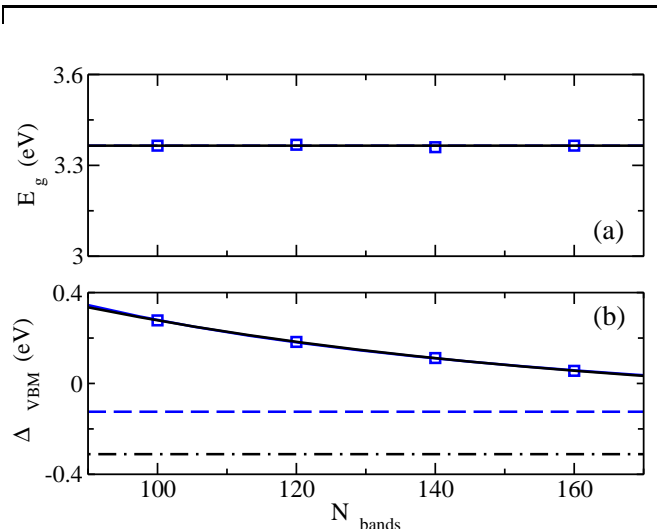


Figure 1: Quasiparticle direct energy gap at Γ (a) and energy of VBM (b) for rutile as a function of the total number of bands kept in the full frequency dependent GW calculation. Squares represent calculations with Ti semi-core electrons included explicitly as valence electrons. The results are fitted using two different functional forms described in the text and displayed as solid lines that are indistinguishable in the figure. However, in (b), they have different $N \rightarrow \infty$ limits, displayed as dash-dot ($1/N$) and long dash ($\exp(-N/c)$) lines in the figure respectively.

tential. In order to characterize the fully converged values, the data were fit with two different empirical forms, $E(N) = E_0 - b/N$, and $E(N) = E_0 - b \cdot \exp(-N/c)$. We first check the validity of the fitting forms for the case of bulk silicon. The exponential form closely represents the band edge and band gap energies as a function of the number of included conduction bands, yielding extrapolated results in excellent agreement with those obtained via methods suggested by Bruneval and Gonze⁷⁵. For rutile, the fitting curves displayed in Fig. 1 are indistinguishable, but predict slightly different $N \rightarrow \infty$ results for the absolute shift of the valence band edge, as indicated by the horizontal dashed lines in Fig. 1(b). In particular, the fit for the quasiparticle energy gap indicates a converged quasiparticle energy of 3.37 eV for $N=160$. For the absolute shift of the valence band edge, the convergence is somewhat slower, with extrapolated values of -0.12 eV and -0.31 eV. This suggests that the valence band edge in the final results is 0.2 to 0.4 eV lower than the $N=160$ value.

C. Bethe-Salpeter Equation and Optical Properties

A detailed description of the BSE method is given in the literature^{27,36}. We use the implementation in

the public branch of the YAMBO package⁷³. With the Tamm-Dancoff approximation⁷⁶ and the use of a static screened Coulomb interaction, the BSE is simplified to a generalized eigenvalue equation $H_{vc,v'c'} A_s^{v'c'} = E_s A_s^{vc}$. The effective Hamiltonian $H_{vc,v'c'}$ has an explicit form of

$$H_{vc,v'c'} = (E_c - E_v) \delta_{vv'} \delta_{cc'} + 2\bar{V}_{vc,v'c'} - \bar{W}_{vc,v'c'}, \quad (6)$$

where the quasiparticle energies (taken from the GW calculations) enter on the diagonal, $\bar{V}_{vc,v'c'} = \langle vc | V_{Coul} | v'c' \rangle$, $\bar{W}_{vc,v'c'} = \langle vv' | W(E=0) | cc' \rangle$ and the indices v, c refer to the occupied valence and empty conduction band states. For brevity, the explicit reference to Bloch wavevector k for each state is suppressed. The effective Hamiltonian in Eq. (6) is explicitly written for the spin singlet excitations which are directly probed in optical measurements. For the spin triplet excitations, the effective Hamiltonian is modified by dropping the so-called exchange term $2\bar{V}_{vc,v'c'}$. In terms of E_s and A_s^{vc} , the macroscopic dielectric function $\epsilon_M(\omega)$, including local field effects^{27,36}, is expressed as

$$\epsilon_M(\omega) = 1 - \lim_{q \rightarrow 0} \frac{4\pi e^2}{q^2} \sum_s \frac{\left| \sum_{vc} \langle v | e^{-i\mathbf{q}\cdot\mathbf{r}} | c \rangle A_s^{vc} \right|^2}{\omega - E_s + i\eta}. \quad (7)$$

In YAMBO, we use the option to evaluate the response function recursively^{73,77}. In order to study specific, low energy exciton states, we also directly diagonalize the generalized eigenvalue equation.

Calculations of optical properties via BSE are more expensive computationally. For both phases, the static dielectric matrices are calculated with 80 bands and a damping coefficient of 0.1 eV. The dielectric function $\epsilon(\omega)$ is calculated on an $8 \times 8 \times 12$ MP mesh for rutile and on an $12 \times 12 \times 12$ MP mesh for anatase. For both cases, electron-hole pairs within 15 eV are taken in to build up the BSE kernel, in which the energy cutoff is 10 Ry for \bar{V} and 3.5 Ry for \bar{W} . To calculate the excitonic binding energy of rutile, we restrict the basis set for the effective Hamiltonian to one conduction band and one valence band. The exciton binding energy converges relatively slowly with BZ sampling. The final results are reported based on a $12 \times 12 \times 18$ MP mesh to sample the BZ. The energy cutoff is larger in this calculation for a more accurate representation of the BSE kernel, 14 Ry for \bar{V} and 6 Ry for \bar{W} .

III. RESULTS

A. Electronic Excitation Energies in TiO₂

The calculated electronic excitation energies in titanium oxides are found to be sensitive to technical factors in the GW calculations. We illustrate that here for the case of TiO₂ in the rutile phase (Table I). First, explicit, self consistent treatment of the semicore electrons

(3s and 3p) on the Ti in the calculations for the solid affects the calculated energy gaps. As discussed in the literature, although the 3s and 3p levels are well separated from the 3d states energetically, there is significant spatial overlap⁶⁹. The effect for TiO₂ is already evident at the LDA level, where the gap is reduced by more than 0.3 eV upon explicit inclusion of the semicore electrons relative to freezing the semicore electrons in the pseudopotential.

Depending on the approximation used to treat the electron self energy in the GW method, the net influence of the semicore electrons varies. Focusing on the influence of the semicore electrons for the most accurate, full-frequency method (FF), the change is greater than 0.3 eV. A more detailed view of the contributions of the LDA exchange-correlation potential V_{xc} , the exchange Σ_x and the correlation Σ_c part of the self energy are also displayed Table I. The valence band maximum (VBM) orbitals are largely composed of oxygen p -states. They are spatially separated from the Ti semicore electrons, so the changes are relatively small. Explicit treatment of the semicore electrons as valence electrons only reduces V_{xc} by 0.24 eV. The reduction in V_{xc} is partially compensated by the decrease of Σ_x (0.08 eV) and Σ_c (0.04 – 0.15 eV). Consequently the overall change of ΔE_{VBM} is less than 0.1 eV. On the other hand, the conduction band minimum (CBM) orbital is almost purely of Ti 3d character with substantial overlap to the semicore electrons. The expectation value of (V_{xc}) changes by about 9 eV. Of course, there is a corresponding, large change in the pseudopotential between these two cases. The bare exchange term in the electron self energy operator changes by a similar amount. Their combined contribution to ΔE_{CBM} is only about -0.34 eV. The changes in the correlation part of the self energy Σ_c of the CBM orbital is sensitive to the GW method. For the full-frequency method, Σ_c is decreased by only 0.1 eV when semicore electrons are included in the PP, so we find that most of the net effect on the band gap comes from the difference between LDA and bare exchange interactions with the semicore electrons.

In Table I the results of using different methods to address the frequency dependence of W are shown. These affect the correlation part of the electron self energy Σ_c and the renormalization factor Z . The results obtained with the full-frequency dependent dielectric function, evaluated using the contour deformation method are the reference results, designated FF(CD) in the table. For comparison, results from two different generalized plasmon pole models are shown. In the Hybertsen-Louie approach²⁴, designated GPP(HL), sum rules are applied to each individual dielectric matrix element to develop a plasmon-pole model for its frequency dependence. As shown in the lower part of Table I, when the semicore electrons of Ti were explicitly included in the pseudopotential, the calculated energy gap is almost 1 eV too large. In the approach of von der Linden and Horsch⁴⁵, designated GPP(VDLH), each dielectric ma-

Method	SC	VBM				CBM				E_g^Γ	
	in PP	V_{xc}	Σ_x	Σ_c	Z	V_{xc}	Σ_x	Σ_c	Z	LDA	GW
GPP(HL)	n	-19.97	-24.59	3.94	0.82	-11.48	-3.57	-5.69	0.84	2.08	4.48
GPP(VDLH)	n	-19.97	-24.59	4.37	0.82	-11.48	-3.57	-6.35	0.85	2.08	3.60
FF(CD)	n	-19.97	-24.59	4.50	0.71	-11.47	-3.57	-5.78	0.73	2.08	3.73
GPP(HL)	y	-20.21	-24.67	4.09	0.83	-20.37	-12.13	-5.64	0.85	1.75	4.27
GPP(VDLH)	y	-20.21	-24.67	4.41	0.83	-20.37	-12.13	-5.99	0.85	1.75	3.70
FF(CD)	y	-20.21	-24.67	4.56	0.70	-20.37	-12.12	-5.88	0.72	1.75	3.38

Table I: Analysis of the valence band maximum (VBM), the conduction band minimum (CBM) and the direct energy gap E_g^Γ at the Γ point of the Brillouin zone calculated for rutile TiO_2 using the GW method with several different approximations. The methods refer to two different generalized plasmon-pole (GPP) models and the full frequency-dependent (FF) approach described in the text. The second column indicates whether Ti semicore states are explicitly included as valence electrons. For the VBM and CBM, the expectation value is shown for the exchange-correlation potential V_{xc} in the LDA, the bare exchange self energy (Σ_x), the correlation part of the self energy (Σ_c) and the renormalization factor (Z). The band gap is shown in the LDA and for the GW method for each case. Energies are given in eV and the renormalization factor Z is dimensionless.

trix is first transformed to the basis of eigenpotentials and then sum rules are applied to develop a plasmon pole model for each eigenpotential. This model also overestimates the energy gap, but by a smaller amount. The renormalization factor Z , in addition to entering the evaluation of the quasiparticle energies in Eq. (3), indicates the degree of dynamical admixture of collective excitations into the quasiparticle. Larger deviations from unity indicate more admixture. Compared with the FF results, the value of Z indicates that the degree of admixture is substantially underestimated by both GPP models.

We have also tested the GPP(HL) approximation for anatase TiO_2 as well as two other titanates, SrTiO_3 and BaTiO_3 . In all three cases, the GPP(HL) approximation leads to minimum band gaps that are too large by 0.7-0.8 eV. A similar deviation for the renormalization constant, Z , is also observed. These results suggest that the quantitative issues with the plasmon pole model extend more generally to titanates. In previous calculations of the loss function⁵⁵ and the finite wavevector dynamical scattering factor⁷⁸ for rutile TiO_2 , substantial structure is seen in the frequency dependence, well beyond what could be easily accounted for by a single pole model. These effects trace to an interplay between strong local field effects and the Ti semicore p- to empty d-shell excitation. However, further analysis of the frequency dependence of the screening in Si and LiCl shows that deviations from a pole model for a range of frequencies around the plasmon energy is not sufficient to predict the performance of the GPP model as it is used to evaluate the GW expression. The dynamical screening at larger frequencies only

K-points	Rutile			Anatase	
	Γ	M	R	Γ	X
E_{LDA}^{Val}	0.00	-1.06	-1.04	-0.48	-0.05
E_{GW}^{Val}	0.00	-1.15	-1.12	-0.58	-0.06
E_{LDA}^{Cond}	1.75	1.80	1.78	1.96	3.22
E_{GW}^{Cond}	3.38	3.40	3.34	3.56	4.89
$E_{gap,GW}^{Direct}$	3.38	4.55	4.45	4.14	4.95
$E_{gap,GW}^{Indirect}$	3.34 ($\Gamma \rightarrow R$)			3.56 ($\Delta \rightarrow \Gamma$)	

Table II: LDA and quasiparticle energy levels of rutile and anatase near the Fermi surface at selected k-points of high symmetry. Corresponding quasiparticle energy gaps are also displayed. The energy reference is taken to be the valence band maximum for both LDA and GW results. All energies are in eV.

enters in an integrated fashion, resulting in substantial cancellations internally. In the case of titanates, we find that the full frequency dependence is essential for quantitative results. Similar conclusions were drawn for the case of metallic Cu⁶⁹.

The quasiparticle energy levels of rutile and anatase from the highest valence band and the lowest conduction band at selected high symmetry k-points are displayed in Table II. While the energy gap of rutile is found to be a direct gap (at Γ) in the LDA, our FF GW calculations indicate it as indirect ($\Gamma \rightarrow R$). However, the energy difference between the direct and indirect gap is small. The energy of CBM at Γ is only 0.04 eV higher than the energy at R .

The calculated quasiparticle energies can be directly compared to spectroscopic measurements for electron removal or addition to the solid. The calculated value of the quasiparticle energy gap, 3.34 eV, agrees well with electron spectroscopy measurements, photo-emission and inverse photo-emission measurements^{46,47}. In Fig. 2, the density of states (DOS) of rutile derived from FF GW calculations is plotted together with the experimental spectra measured using x-ray photoemission and bremsstrahlung isochromat spectroscopy⁴⁶, which yielded a band gap of 3.3 ± 0.5 eV. Overall, the shape of the calculated DOS matches the shape of the experimental spectra, especially around the band gap. The experimental spectra measured using ultraviolet photoemission and inverse photoemission spectroscopy⁴⁷ show very similar results with the inferred minimum energy gap about 0.2 eV smaller.

The LDA calculations show that the top of the valence band of anatase lies in the Δ direction, somewhere about 0.88 times of the distance from Γ to X . The energy at this k-point is 0.05 eV higher than the energy of the VBM at X . Subtracting the energy difference as a perturbation from the quasiparticle energy gap between X and Γ , which is 3.62 eV from Table II, the quasiparticle energy gap of anatase is found to be 3.56 eV. The photoemission data available for anatase show an overall occupied band with the oxygen p-bands⁷⁹. That is similar to rutile. To our knowledge, there is no inverse photoemission data available for anatase, so the calculations can not be compared to a direct measurement of the quasiparticle energy gap.

B. Optical Excitation Energies in TiO_2

More precise measurements of the minimum energy gap rely on optical absorption. This introduces the extra complication that the observed threshold for absorption will be altered by interactions between the photoexcited electron and hole, the formation of bound exciton states. For rutile, the BSE calculation shows a series of singlet bound excitonic states at Γ . The lowest two show s -state symmetry in the electron-hole envelope. They have a binding energy of 0.13 eV and 0.06 eV respectively. They are not dipole-allowed. The third and fourth are degenerate, with electron-hole envelope showing $p_{x,y}$ symmetry, and have a binding energy of 26 meV. They are weakly dipole allowed for the electric vector perpendicular to the c -axis. Together with the calculated direct quasipar-

ticle gap energy from above, we obtain the lowest energy singlet exciton at Γ with energy 3.25 eV and the first dipole allowed singlet exciton with energy of 3.35 eV. High resolution, low temperature optical absorption measurements for rutile resolve several separate features¹⁸. A very weak, but sharp exciton feature at 3.031 eV is identified as the 1s exciton which is electric quadrupole allowed. A stronger, but still relatively weak, dipole allowed 2p exciton feature starts at 3.034 eV. Finally, phonon-assisted features are also identified that correspond to an indirect gap of 3.049 eV.

There are several important points of comparison. First, the calculated lowest exciton energy at Γ is about 0.22 eV higher than measured. Broadly, this error is comparable to those encountered when using the GW approximation for other semiconductors²⁵⁻²⁷. However, it is important to be clear that the calculation is performed for a frozen lattice with no account given for electron-phonon interactions. In general, the electron-phonon interaction will reduce the zero-temperature quasiparticle gap⁸⁰. Second, the present GW calculation gives the conduction band minimum at the R point instead of being at Γ , as suggested by the optical measurements. The energy differences are small; the calculated conduction band at R is 0.04 eV lower than at Γ . In the analysis of the absorption data, the indirect gap is found to be 0.01 eV higher than the direct gap¹⁸, albeit including what ever role excitonic effects may have. The difference between theory and experiment is too subtle to be resolved in these calculations, particularly without the influence of electron-phonon interactions. Third, the symmetry of the excitonic states from the calculation agrees with the interpretation of the experiments. However, the scale of the excitonic effects that we calculate using the static dielectric matrix, and only including the electronic polarizability, is substantially larger than suggested by the experiment. Our calculated long-wavelength dielectric constant (~ 8) is slightly higher than the measured ϵ_∞ (~ 7)³⁴, but similar to previous calculations⁵⁵. The lattice contribution is quite large, with $\epsilon_0 = 111$ ¹⁸. This again points to the importance of the electron-phonon interaction.

The measured optical absorption in single crystal anatase at low temperature does not resolve any significant structure⁸¹. The energy dependence near the onset of absorption is consistent with an Urbach tail. Analysis of the temperature dependence leads to an estimate for the band gap for extended states of 3.42 eV⁸¹. This exceeds the measured optical threshold in rutile by about 0.4 eV. Since the measured absorption edge in anatase is featureless, another way to characterize the absorption edge and make comparison to rutile is to consider the energy at which the low temperature absorption is 50 cm^{-1} for electric vector perpendicular to the c -axis. In rutile, this occurs at 3.04 eV while it occurs at 3.30 eV in anatase⁸¹. This suggests a more modest 0.26 eV difference between the minimum energy gap of anatase and rutile. Our calculated quasiparticle minimum energy

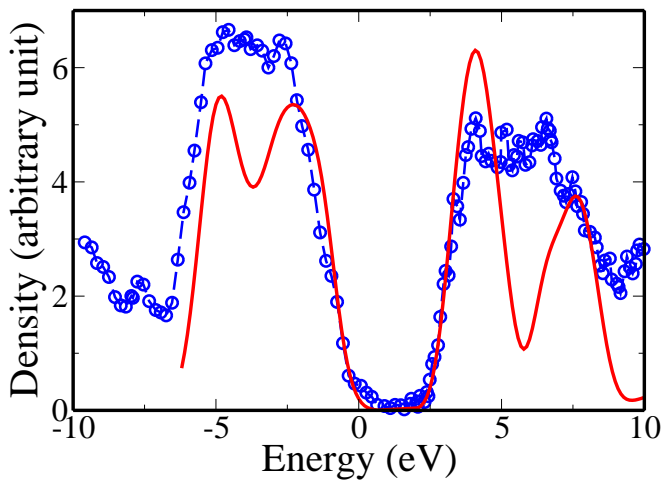


Figure 2: Density of states (DOS) of rutile derived from FF GW calculations plotted with photoemission and inverse photoemission spectra⁴⁶. The solid curve is the calculated DOS which is convoluted with a Gaussian function of $\sigma = 0.5$ eV, while circles are photo- and inverse photo-emission spectra.

gap in anatase is 3.56 eV, modestly larger than the value deduced from the absorption measurements. The calculated difference in gaps between anatase and rutile is 0.22 eV, similar to the measured difference.

So far, the calculated quasiparticle energies for TiO_2 have been found to agree well with electron spectroscopy, but the minimum energy gaps, including excitonic effects, are larger compared to the measured absorption threshold. Furthermore, the strength of the calculated exciton binding energy is larger than implied by the interpretation of the optical spectrum near threshold. To get additional perspective, we calculate the macroscopic dielectric function over a broad energy range, including the correlations induced by electron-hole interactions.

In Fig. 3, we show the imaginary part of the dielectric function of rutile for polarizations both perpendicular and parallel to the tetragonal axis c . The solid curves are calculated from the BSE, while the dashed curves are derived from optical reflectivity measurements at room temperature³⁴. For both polarizations, the theoretical spectra are close to experiment up to about 6 eV. In particular, the first strong peak at ~ 4 eV for both polarizations is reproduced very well by the BSE results. Above 6 eV, the overall magnitude and prominence of the peaks in theoretical spectra are distinct from experiment. The $\epsilon_2(\omega)$ of anatase is displayed in Fig. 4, where the experimental data³⁵ were measured at 100 K. Similar to the rutile case, the theoretical calculations capture the features around the onset of major absorption at 4 eV. For perpendicular polarization, the calculated oscillator strength is systematically too large starting at about 5 eV. The calculated results are very similar to the previous calculation for rutile TiO_2 ³⁷. For anatase, the calculated peak heights near 4 eV appear less intense in their spectra, but this is largely due to their choice of a larger

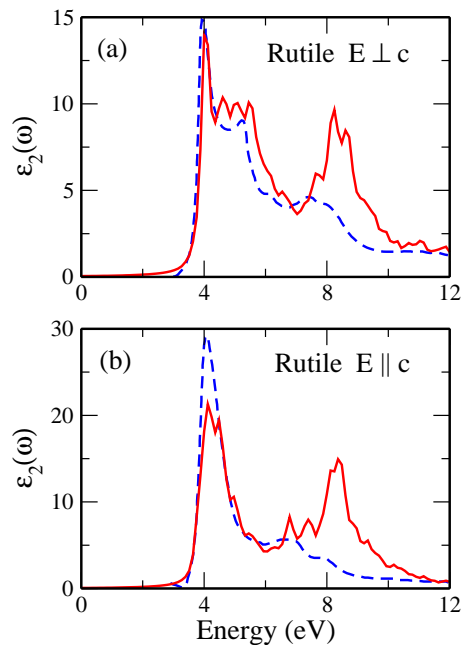


Figure 3: $\epsilon_2(\omega)$ of rutile from 0 to 12 eV. Solid curves are theoretical calculations with BSE, and dashed curves are experimental results³⁴ obtained at room temperature. In (a) the direction of polarization is perpendicular to the tetragonal axis c , and in (b) the direction of polarization is parallel to axis c .

damping parameter, as is evident from the broadening on the low energy side of their spectra. In particular, we have analyzed the integrated oscillator strength (i.e. the contribution to the f-sum rule) from the first peak in the anatase spectrum for parallel polarization. We find that our oscillator strength is essentially the same as theirs, but that both calculations show more oscillator strength than is found in the experimental spectra by about 30%.

The systematic overestimation of oscillator strength at higher energy appears to be a more general issue. For example, a recent BSE study for several alkaline earth metal monoxides shows some similar excess oscillator strength at higher photon energies⁸². This may well trace to more fundamental assumptions in the methodology. Two key issues are the use of the Tamm-Dancoff approximation, which has been identified recently as the main source of errors in the calculations of a confined system⁸³, and the assumption of a statically screened Coulomb interaction^{36,84}. Also, as noted by Lawler and coworkers, the f-sum rule for the oscillator strength converges very slowly in the titanates and the experimental analysis that relies on Kramers-Kronig transformations may have systematic errors as well³⁷.

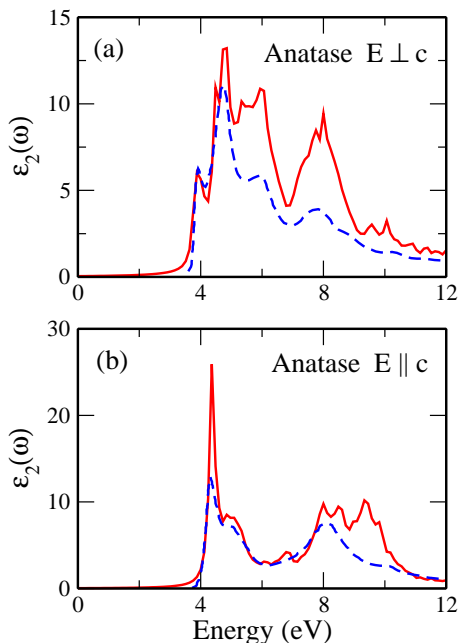


Figure 4: $\epsilon_2(\omega)$ of anatase from 0 to 12 eV. Solid curves are theoretical calculations from BSE, and dashed curves are experimental results obtained at 100K³⁵. In (a) the direction of polarization is perpendicular to the tetragonal axis c , and in (b) the direction of polarization is parallel to axis c .

C. External Energy Level Alignment: $\text{TiO}_2(110)$ Surface

The energetic position of the quasiparticle VBM with respect to the vacuum level in the rutile phase for the (110) surface was calculated in several steps. First at the LDA level, analogous to the determination of work function for metals, the electrostatic potential change between the bulk like region and the vacuum region was determined^{85–88}. Then in a second step, the bulk VBM position relative to the electrostatic potential is determined. Previous calculations of work functions based on metal slabs based on the DFT Fermi energy were in fairly good agreements with experimental measurements^{89,90}. In the third step, we will apply the perturbative correction to the LDA exchange-correlation potential to determine the alignment in the GW approximation^{85,88}.

For semiconductors and insulators the Fermi level is separated from the VBM, and the position of VBM varies as the surface structure changes. To calculate the energetic alignment of rutile with respect to the vacuum from the (110) surface, a stoichiometric slab of six layers of Ti atoms is cut from the bulk structure with geometrical parameters described in Sec. I. A vacuum space of the same thickness of the slab is used to buffer the two surfaces of the slab. The surface is cleaved as a (1×1) , unreconstructed surface as observed in experiments². The k -point mesh is $2 \times 4 \times 1$. After the slab is fully relaxed with the atomic positions of the central two layers fixed,

the electrostatic potential inside the slab with respect to the vacuum is measured as -12.65 eV. The energy difference between the VBM (from the LDA calculation) and the electrostatic potential inside the material is 5.05 eV, which is determined in a separate bulk calculation to prevent the quantum size effects⁸⁹. Accordingly, the LDA value for the VBM relative to vacuum is 7.60 eV. Previous LDA and gradient corrected calculations for give 7.16 eV (LDA, three Ti layer slab)⁹¹, 7.2 eV (PBE, 11 Ti layer slab)⁹² and 7.6 eV (PW91, 11 Ti layer slab)⁹². In light of variations at the 0.2 eV level with number of layers in the slab model⁹², the overall agreement is satisfactory.

The GW correction for the VBM calculated with FF model and 160 bands is 0.07 eV. However, as noted in Sect. IIC, extrapolation to full convergence with respect to the total number of bands will drive this 0.2 to 0.4 eV lower. We therefore suggest a GW correction of -0.2 eV, with about 0.1 eV uncertainty. The final prediction from GW for the VBM alignment to vacuum at the clean rutile $\text{TiO}_2(110)$ surface is 7.8 eV.

In order to deduce the VBM alignment from experiment, two results must be combined: (1) the work function which fixes the Fermi energy relative to the vacuum; (2) the position of the VBM relative to the Fermi energy. Experimental measurements of the work function of rutile from the (110) surface^{93,94} vary from 4.7 eV to 5.8 eV depending on the structure of the surface which is strongly influenced by treatment (annealing, exposure to oxygen, etc.). In addition, the position of the VBM relative to the Fermi energy also depends on surface treatment⁹⁵. Therefore, it is crucial to compare with data in which both values are measured on the same sample. To our knowledge, this is relatively rare. Based on UPS measurements with ($h\nu=21.2$ eV), a work function of 5.2 eV and a relative VBM position of 3 eV were measured for $\text{TiO}_2(110)$ ⁹⁴, which implies the VBM position relative to vacuum falls at 8.2 eV. Similar measurements for $\text{TiO}_2(100)$ yield a work function of 4.9 eV and a relative VBM position of 3.1 eV respectively⁹⁶, yielding the VBM position at 8.0 eV. The difference in workfunction between these measurements is consistent with a separate Auger Microprobe study of facet dependence⁹⁷.

Based on this limited data set, the GW based prediction for the VBM alignment is off by about 0.4 eV. There are at least 0.1 eV uncertainties in both the theory and the experiment. Since both the work function and position of Fermi level are sensitive to the surface properties, the deviation between the theoretical calculation and experimental measurements may well reflect the complexity of the TiO_2 surfaces. For example, recent studies suggest that the commonly employed strategy of cleaning followed by annealing in oxygen may not result in the ideal surface envisioned (e.g. with no oxygen related defects)⁹⁵. In particular, the physical origin of the widely observed defect states around 1 eV below the CBM remains a point of vigorous discussion^{95,98}.

IV. CONCLUDING REMARKS

We have presented a numerically well converged MBPT study of the electronic and optical excitation energies in rutile and anatase crystals of TiO_2 . The calculations are carried out in the approximation of a frozen lattice, without consideration of electron-phonon coupling. In most respects, the agreement with experiment is well within the expected accuracy of this approach. In particular, the calculated quasiparticle gap agrees with electron spectroscopy measurements (photoemission and inverse photoemission), the change in the minimum gap between rutile and anatase crystal structures is reproduced, and the main features of the optical spectrum agree with ellipsometry measurements. The qualitative features of the zone center bound excitons calculated for rutile agree well with low temperature absorption measurements. However, the scale of the exciton binding energy is larger than that estimated from experiment by about a factor of 10 and the calculated exciton energy is about 0.2 eV larger than measured.

The key theoretical assumptions in our application of MBPT include evaluation of the electron self energy in the GW approximation without iterating to self consistency or considering vertex corrections. Self consistency would certainly increase the calculated energy gap through the reduction in the screening^{29,44}. Recent results for a set of other semiconductors and insulators shows that approximate inclusion of vertex corrections in screening leads to a partially compensating reduction of the calculated energy gap⁴³. However, a fully consistent approach to include vertex corrections remains subject of current research in the field. Because the Ti $3d$ electrons are almost completely ionized, TiO_2 should not be subject to the sorts of systematic errors found in non-selfconsistent calculations for some late transition $3d$ metal compounds^{61–63}. The accurate results found for the key optical transition energies contributing to the absorption (Figs. 3 and 4) support this, and contrast to the case of Cu_2O where non-selfconsistent calculations showed substantial discrepancies⁶³. In the solution of the BSE, the calculated static (electronic) dielectric matrix has been used and the equations were simplified through the Tamm-Dancoff approximation. These approximations are part of the standard MBPT treatment of optical spectra and the low energy excitons are expected to be treated well^{27,36}. However, they may affect higher energy features in the spectra⁸⁴.

On physical grounds, we suggest that the most significant open issue concerns the role of electron-phonon coupling. In general, the electron-phonon self energy will both lead to a smaller zero-temperature quasiparticle gap and make a significant contribution to the temperature dependence of the energy gap⁸⁰. As noted in the text, there is a very large difference between the electronic dielectric constant ϵ_∞ and the low frequency dielectric constant including lattice polarization ϵ_0 for TiO_2 . This suggests a relatively strong electron-phonon interaction

and there is a long standing debate over the polaronic character of charge excitations in TiO_2 ⁹⁹.

Based on the usual form of the Frohlich interaction, the dimensionless coupling constant characterizing electronic coupling to the most important polar optic mode for rutile (with mode energy about 0.1 eV) is given by $\alpha = 1.6\sqrt{m_b/m_e}$ where m_b is the bare band mass and m_e is the free electron mass. Using our DFT band dispersions to have estimates, the electron (hole) band mass is about $0.6m_e$ ($1.8m_e$) along x or y and $1.6m_e$ ($3.1m_e$) along z . This suggests coupling constants of $\alpha \sim 1 - 2$ for electrons and $\alpha \sim 2 - 3$ for holes which would fall in the weak to intermediate coupling regime. Using the usual weak coupling expression, the electron and hole renormalization would be 0.1 – 0.2 eV and 0.2 – 0.3 eV respectively, both of which act to reduce the quasiparticle energy gap. For anatase $\alpha \sim 1.6\sqrt{m_b/m_e}$, essentially the same as rutile, based on the mode energy and dielectric constants¹⁰⁰. The electron (hole) band mass is about $0.4m_e$ ($1.8m_e$) along x or y and $3.9m_e$ ($1.0m_e$) along z , suggesting slightly different coupling constants of $\alpha \sim 1 - 3$ for electrons and $\alpha \sim 2$ for holes with corresponding (weak coupling) electron and hole renormalization of 0.1-0.3 eV and 0.2 eV respectively. In weak coupling, the electron-phonon self energy is added to the results obtained here based on the GW approximation. For the analysis of the optical absorption edge, a more detailed calculation is required because in the exciton-phonon coupling, the exciton is neutral and the electron and hole distortions of the lattice will partially cancel^{101,102}. Taken together, if the large polaron regime is physically correct, these rough estimates suggest that the effect of the electron-phonon coupling could account for some of the differences between the present GW/BSE results for the frozen lattice and experiment. Firmer conclusions require a more extensive set of calculations, beyond the scope of this article^{80,103–105}. In particular, it may be that a more complete consideration of self-consistency and vertex corrections in the electron-electron contribution to the electron self energy will need to be combined with an analysis of the electron-phonon contribution. The two contributions should be treated in a fully consistent theory. In more empirical terms, an overestimate of the band gap based on selfconsistent treatment of the electron-electron interactions alone may be compensated by the electron-phonon contributions.

It may well be the case that the large polaron regime is not applicable for TiO_2 . A recent THz spectroscopy study of rutile gave a direct measurement of the electron scattering rate¹⁰⁶. This data was analyzed with a Frohlich form for the electron-phonon interaction, but regarding the coupling constant as a free parameter. Using the Feynman approach^{107,108} to handle intermediate to strong coupling, the analysis showed coupling constants for electrons $\alpha \sim 4 - 6$ depending on field orientation¹⁰⁶. The inferred electron mobilities were consistent with earlier electron transport measurements¹⁰⁹. These values suggest a substantially larger value for the electron self

energy of $0.4 - 0.7$ eV¹⁰⁸. An older estimate based on small polaron theory also suggested 0.7 eV¹¹⁰. A recent DFT+U based study suggested that an excess electron in rutile is indeed self trapped¹¹¹. Although the binding energy was not presented, the barrier for polaron hopping was estimated to be 0.3 eV. A similar study for an excess hole in rutile suggested barriers of $0.5 - 0.6$ eV¹¹². Taken together, if the small polaron regime is found to be physically relevant, then the quasiparticle and excitonic energies will need to be fully reanalyzed. For strong electron-phonon coupling a perturbative approach to combine the electron-electron and electron-phonon self energies is no longer justified. Furthermore, the electron-phonon coupling enters into the spectroscopic measurements in distinct ways. The (inverse) photoemission and optical absorption would each need to be properly analyzed.

Acknowledgments

We thank Dr. A. Marini for access to the private branch of the Yambo code. W. K. thanks Dr. D. Prezzi for insightful discussions on BSE. Work performed under the auspices of the U.S. Department of Energy under Contract No. DEAC02-98CH1-886. This research utilized resources at the New York Center for Computational Sciences at Stony Brook University/Brookhaven National Laboratory which is supported by the U.S. Department of Energy under Contract No. DE-AC02-98CH10886 and by the State of New York.

-
- ¹ F. A. Grant, *Rev. Mod. Phys.* **31**, 646 (1959).
² U. Diebold, *Surf. Sci. Rep.* **48**, 53 (2003).
³ M. A. Fox and M. T. Dulay, *Chem. Rev.* **93**, 341 (1993).
⁴ M. R. Hoffmann, S. T. Martin, W. Choi, and D. W. Bahnmann, *Chem. Rev.* **95**, 69 (1995).
⁵ A. Fujishima and K. Honda, *Nature* **238**, 37 (1972).
⁶ B. Oregan and M. Gratzel, *Nature* **353**, 737 (1991).
⁷ L. Pauling, *J. Am. Chem. Soc.* **51**, 1010 (1929).
⁸ S. C. Abrahams and J. L. Bernstein, *J. Chem. Phys.* **55**, 3206 (1971).
⁹ M. Horn, C. F. Schwerdtfeger, and E. P. Meagher, *Z. Kristallogr.* **136**, 273 (1972), as cited in¹⁰.
¹⁰ A. Fahmi, C. Minot, B. Silvi, and M. Causá, *Phys. Rev. B* **47**, 11717 (1993).
¹¹ J. K. Burdett, T. Hughbanks, G. J. Miller, J. W. Richardson, and J. V. Smith, *J. Am. Chem. Soc.* **109**, 3639 (1987).
¹² P. Hohenberg and W. Kohn, *Phys. Rev.* **136**, B864 (1964).
¹³ W. Kohn and L. J. Sham, *Phys. Rev.* **140**, A1133 (1965).
¹⁴ K. M. Glassford and J. R. Chelikowsky, *Phys. Rev. B* **46**, 1284 (1992).
¹⁵ S.-D. Mo and W. Y. Ching, *Phys. Rev. B* **51**, 13023 (1995).
¹⁶ M. Mikami, S. Nakamura, O. Kitao, H. Arakawa, and X. Gonze, *Jpn. J. Appl. Phys.* **39**, L847 (2000).
¹⁷ R. Asahi, Y. Taga, W. Mannstadt, and A. J. Freeman, *Phys. Rev. B* **61**, 7459 (2000).
¹⁸ J. Pascual, J. Camassel, and H. Mathieu, *Phys. Rev. Lett.* **39**, 1490 (1977).
¹⁹ H. Tang, H. Berger, P. Schmid, F. Lévy, and G. Burri, *Solid State Commun.* **87**, 847 (1993).
²⁰ Y.-f. Zhang, W. Lin, Y. Li, K.-n. Ding, and J.-q. Li, *J. Phys. Chem. B* **109**, 19270 (2005).
²¹ J. Muscat, A. Wander, and N. M. Harrison, *Chem. Phys. Lett.* **342**, 397 (2001).
²² M. Nolan, S. D. Elliott, J. S. Mulley, R. A. Bennett, M. Basham, and P. Mulheran, *Phys. Rev. B* **77**, 235424 (2008).
²³ L. Hedin, *Phys. Rev.* **139**, A796 (1965).
²⁴ M. S. Hybertsen and S. G. Louie, *Phys. Rev. B* **34**, 5390 (1986).
²⁵ F. Aryasetiawan and O. Gunnarsson, *Rep. Prog. Phys.* **61**, 237 (1998).
²⁶ W. G. Aulbur, L. Jönsson, and J. W. Wilkins, *Solid State Phys.* **54**, 1 (1999).
²⁷ G. Onida, L. Reining, and A. Rubio, *Rev. Mod. Phys.* **74**, 601 (2002).
²⁸ M. Oshikiri, M. Boero, J. Ye, F. Aryasetiawan, and G. Kido, *Thin Solid Films* **445**, 168 (2003).
²⁹ M. van Schilfgaarde, T. Kotani, and S. Faleev, *Phys. Rev. Lett.* **96**, 226402 (2006).
³⁰ L. Thulin and J. Guerra, *Phys. Rev. B* **77**, 195112 (2008).
³¹ D. J. Mowbray, J. I. Martinez, J. M. García Lastra, K. S. Thygesen, and K. W. Jacobsen, *J. Phys. Chem. C* **113**, 12301 (2009).
³² K. M. Glassford and J. R. Chelikowsky, *Phys. Rev. B* **45**, 3874 (1992).
³³ H. Ehrenreich and M. H. Cohen, *Phys. Rev.* **115**, 786 (1959).
³⁴ M. Cardona and G. Harbeke, *Phys. Rev.* **137**, A1467 (1965).
³⁵ N. Hosaka, T. Sekiya, C. Satoko, and S. Kurita, *J. Phys. Soc. Jpn.* **66**, 877 (1997).
³⁶ M. Rohlfing and S. G. Louie, *Phys. Rev. B* **62**, 4927 (2000).
³⁷ H. M. Lawler, J. J. Rehr, F. Vila, S. D. Dalosto, E. L. Shirley, and Z. H. Levine, *Phys. Rev. B* **78**, 205108 (2008).
³⁸ E. L. Shirley, *Phys. Rev. B* **54**, 7758 (1996).
³⁹ B. Holm and U. von Barth, *Phys. Rev. B* **57**, 2108 (1998).
⁴⁰ W. Ku and A. G. Eguiluz, *Phys. Rev. Lett.* **89**, 126401 (2002).
⁴¹ F. Bruneval, N. Vast, and L. Reining, *Phys. Rev. B* **74**, 045102 (2006).
⁴² T. Kotani, M. van Schilfgaarde, and S. V. Faleev, *Phys. Rev. B* **76**, 165106 (2007).
⁴³ M. Shishkin, M. Marsman, and G. Kresse, *Phys. Rev. Lett.* **99**, 246403 (2007).
⁴⁴ M. Shishkin and G. Kresse, *Phys. Rev. B* **75**, 235102 (2007).
⁴⁵ W. von der Linden and P. Horsch, *Phys. Rev. B* **37**, 8351 (1988).
⁴⁶ Y. Tezuka, S. Shin, T. Ishii, T. Ejima, S. Suzuki, and S. Sato, *J. Phys. Soc. Jpn.* **63**, 347 (1994).
⁴⁷ A. K. See and R. A. Bartynski, *Phys. Rev. B* **50**, 12064 (1994).

- ⁴⁸ X. Gonze, J. M. Beuken, R. Caracas, F. Detraux, M. Fuchs, G. M. Rignanese, L. Sindic, M. Verstraete, G. Zerah, F. Jollet, et al., *Comput. Mater. Sci.* **25**, 478 (2002).
- ⁴⁹ X. Gonze, G. M. Rignanese, M. Verstraete, J. M. Beuken, Y. Pouillon, R. Caracas, F. Jollet, M. Torrent, G. Zerah, M. Mikami, et al., *Zeitschrift Fur Kristallographie* **220**, 558 (2005).
- ⁵⁰ URL <http://opium.sourceforge.net/>.
- ⁵¹ N. Troullier and J. L. Martins, *Phys. Rev. B* **43**, 1993 (1991).
- ⁵² M. Fuchs and M. Scheffler, *Comput. Phys. Commun.* **119**, 67 (1999).
- ⁵³ J. P. Perdew and Y. Wang, *Phys. Rev. B* **45**, 13244 (1992).
- ⁵⁴ D. M. Ceperley and B. J. Alder, *Phys. Rev. Lett.* **45**, 566 (1980).
- ⁵⁵ N. Vast, L. Reining, V. Olevano, P. Schattschneider, and B. Joffrey, *Phys. Rev. Lett.* **88**, 037601 (2002).
- ⁵⁶ G. Kresse and J. Furthmüller, *Comput. Mater. Sci.* **6**, 15 (1996).
- ⁵⁷ G. Kresse and J. Furthmüller, *Phys. Rev. B* **54**, 11169 (1996).
- ⁵⁸ P. E. Blöchl, *Phys. Rev. B* **50**, 17953 (1994).
- ⁵⁹ D. T. Cromer and K. Herrington, *J. Am. Chem. Soc.* **77**, 4708 (1955).
- ⁶⁰ L. Hedin and S. Lundqvist, *Solid State Phys.* **23**, 1 (1969).
- ⁶¹ F. Aryasetiawan and O. Gunnarsson, *Phys. Rev. Lett.* **74**, 3221 (1995).
- ⁶² S. V. Faleev, M. van Schilfgaarde, and T. Kotani, *Phys. Rev. Lett.* **93**, 126406 (2004).
- ⁶³ F. Bruneval, N. Vast, L. Reining, M. Izquierdo, F. Sirotti, and N. Barrett, *Phys. Rev. Lett.* **97**, 267601 (2006).
- ⁶⁴ M. S. Hybertsen and S. G. Louie, *Phys. Rev. B* **32**, 7005 (1985).
- ⁶⁵ E. L. Shirley, *Phys. Rev. B* **58**, 9579 (1998).
- ⁶⁶ H. N. Rojas, R. W. Godby, and R. J. Needs, *Phys. Rev. Lett.* **74**, 1827 (1995).
- ⁶⁷ M. M. Rieger, L. Steinbeck, I. White, H. Rojas, and R. Godby, *Comput. Phys. Commun.* **117**, 211 (1999).
- ⁶⁸ A. Marini, R. D. Sole, A. Rubio, and G. Onida, *Phys. Rev. B* **66**, 161104(R) (2002).
- ⁶⁹ A. Marini, G. Onida, and R. D. Sole, *Phys. Rev. Lett.* **88**, 016403 (2002).
- ⁷⁰ M. Shishkin and G. Kresse, *Phys. Rev. B* **74**, 035101 (2006).
- ⁷¹ S. Lebègue, B. Arnaud, M. Alouani, and P. E. Bloechl, *Phys. Rev. B* **67**, 155208 (2003).
- ⁷² F. Bruneval, Ph.D. thesis, Ecole Polytechnique, Palaiseau, France (2005), URL http://theory.lsi.polytechnique.fr/people/bruneval/bruneval_these.pdf.
- ⁷³ A. Marini, C. Hogan, M. Grüning, and D. Varsano, *Comput. Phys. Commun.* **180**, 1392 (2009).
- ⁷⁴ H. J. Monkhorst and J. D. Pack, *Phys. Rev. B* **13**, 5188 (1976).
- ⁷⁵ F. Bruneval and X. Gonze, *Phys. Rev. B* **78**, 085125 (2008).
- ⁷⁶ A. L. Fetter and J. D. Walecka, *Quantum Theory of Many-Particle Systems* (McGraw-Hill, 1971).
- ⁷⁷ L. X. Benedict and E. L. Shirley, *Phys. Rev. B* **59**, 5441 (1999).
- ⁷⁸ I. G. Gurtubay, W. Ku, J. M. Pitarke, A. G. Eguluz, B. C. Larson, J. Tischler, and P. Zschack, *Phys. Rev. B* **70**, 201201 (2004).
- ⁷⁹ R. Sanjinés, H. Tang, H. Berger, F. Gozzo, G. Margari-
tondo, and F. Lévy, *J. Appl. Phys.* **75**, 2945 (1994).
- ⁸⁰ M. Cardona and M. L. W. Thewalt, *Rev. Mod. Phys.* **77**, 1173 (2005).
- ⁸¹ H. Tang, F. Lévy, H. Berger, and P. E. Schmid, *Phys. Rev. B* **52**, 7771 (1995).
- ⁸² A. Schleife, C. Rodl, F. Fuchs, J. Furthmüller, and F. Bechstedt, *Phys. Rev. B* **80**, 035112 (2009).
- ⁸³ M. Grüning, A. Marini, and X. Gonze, *Nano Lett.* **9**, 2820 (2009).
- ⁸⁴ A. Marini and R. Del Sole, *Phys. Rev. Lett.* **91**, 176402 (2003).
- ⁸⁵ S. B. Zhang, D. Tomanek, S. G. Louie, M. L. Cohen, and M. S. Hybertsen, *Solid State Commun.* **66**, 585 (1988).
- ⁸⁶ A. Baldereschi, S. Baroni, and R. Resta, *Phys. Rev. Lett.* **61**, 734 (1988).
- ⁸⁷ C. J. Fall, N. Binggeli, and A. Baldereschi, *J. Phys.: Condens. Matter* **11**, 2689 (1999).
- ⁸⁸ R. Shaltaf, G. M. Rignanese, X. Gonze, F. Giustino, and A. Pasquarello, *Phys. Rev. Lett.* **100**, 186401 (2008).
- ⁸⁹ C. J. Fall, N. Binggeli, and A. Baldereschi, *Phys. Rev. B* **58**, R7544 (1998).
- ⁹⁰ C. J. Fall, N. Binggeli, and A. Baldereschi, *Phys. Rev. B* **61**, 8489 (2000).
- ⁹¹ D. Vogtenhuber, R. Podloucky, J. Redinger, E. L. D. Hebenstreit, W. Hebenstreit, and U. Diebold, *Phys. Rev. B* **65**, 125411 (2002).
- ⁹² A. Kiejna, T. Pabisiak, and S. W. Gao, *J. Phys.: Condens. Matter* **18**, 4207 (2006), and reference herein.
- ⁹³ K. Onda, B. Li, and H. Petek, *Phys. Rev. B* **70**, 045415 (2004).
- ⁹⁴ K. D. Schierbaum, S. Fischer, M. C. Torquemada, J. L. de Segovia, E. Román, and J. A. Martín-Gago, *Surf. Sci.* **345**, 261 (1996).
- ⁹⁵ S. Wendt, P. T. Sprunger, E. Lira, G. K. H. Madsen, Z. Li, J. O. Hansen, J. Matthiesen, A. Blekinge-Rasmussen, E. Laegsgaard, B. Hammer, et al., *Science* **320**, 1755 (2008).
- ⁹⁶ G. Xiong, R. Shao, T. Droubay, A. Joly, K. Beck, S. Chambers, and W. Hess, *Adv. Funct. Mater.* **17**, 2133 (2007).
- ⁹⁷ A. Imanishi, E. Tsuji, and Y. Nakato, *J. Phys. Chem. C* **111**, 2128 (2007).
- ⁹⁸ C. Di Valentin, G. Pacchioni, and A. Selloni, *Phys. Rev. Lett.* **97**, 166803 (2006).
- ⁹⁹ Detailed references can be found in the papers cited below^{106,109–112}.
- ¹⁰⁰ R. J. Gonzalez, R. Zallen, and H. Berger, *Phys. Rev. B* **55**, 7014 (1997).
- ¹⁰¹ S. Schmitt-Rink, D. A. B. Miller, and D. S. Chemla, *Phys. Rev. Lett.* **58**, 813 (1987).
- ¹⁰² S. Rudin, T. L. Reinecke, and B. Segall, *Phys. Rev. B* **42**, 11218 (1990).
- ¹⁰³ A. Marini, *Phys. Rev. Lett.* **101**, 106405 (2008).
- ¹⁰⁴ F. Bechstedt, K. Seino, P. H. Hahn, and W. G. Schmidt, *Phys. Rev. B* **72**, 245114 (2005).
- ¹⁰⁵ J. Vidal, F. Trani, F. Bruneval, M. A. L. Marques, and S. Botti, *Phys. Rev. Lett.* **104**, 136401 (2010).
- ¹⁰⁶ E. Hendry, F. Wang, J. Shan, T. F. Heinz, and M. Bonn, *Phys. Rev. B* **69**, 081101 (2004).
- ¹⁰⁷ R. P. Feynman, *Phys. Rev.* **97**, 660 (1955).
- ¹⁰⁸ T. D. Schultz, *Phys. Rev.* **116**, 526 (1959).
- ¹⁰⁹ E. Yagi, R. R. Hasiguti, and M. Aono, *Phys. Rev. B* **54**, 7945 (1996).
- ¹¹⁰ D. Eagles, *J. Phys. Chem. Solids* **25**, 1243 (1964).

- ¹¹¹ N. A. Deskins and M. Dupuis, Phys. Rev. B **75**, 195212 (2007).
- ¹¹² N. A. Deskins and M. Dupuis, J. Phys. Chem. C **113**, 346